Electrochemical Measurements of Single H 2 Nanobubble Nucleation and Stability at Pt Nanoelectrodes

ARTICLE *in* JOURNAL OF PHYSICAL CHEMISTRY LETTERS · SEPTEMBER 2014

Impact Factor: 7.46 · DOI: 10.1021/jz501898r

THE JOURNAL OF PHYSICAL CHEMISTRY Letters

Letter

pubs.acs.org/JPCL

Electrochemical Measurements of Single H_2 Nanobubble Nucleation and Stability at Pt Nanoelectrodes

Qianjin Chen,[†] Long Luo,[†] Hamaseh Faraji,[†] Stephen W. Feldberg,[‡] and Henry S. White*[,†]

[†]Department of Chemistry, University of Utah, 315 S 1400 E, Salt Lake City, Utah 84112, United States

[‡]Chemistry Department, Brookhaven National Laboratory, Upton, New York 11973, United States

Supporting Information

ABSTRACT: Single H_2 nanobubble nucleation is studied at Pt nanodisk electrodes of radii less than 50 nm, where H_2 is produced through electrochemical reduction of protons in a strong acid solution. The critical concentration of dissolved H_2 required for nanobubble nucleation is measured to be ~0.25 M. This value is ~310 times larger than the saturation concentration at room temperature and pressure and was found to be independent of acid type (e.g., H_2SO_4, HCl, and H_3PO_4) and nanoelectrode size. The effects of different surfactants on H_2 nanobubble nucleation are consistent with the classic nucleation theory. As the surfactant concentration in H_2SO_4 solution increases, the solution surface tension decreases, resulting in a lower nucleation energy barrier and consequently a lower supersaturation concentration required for H_2 nanobubble nucleation. Furthermore, amphiphilic surfactant molecules accumulate at the H_2/solution interface, hindering interfacial H_2 transfer from the nanobubble into the solution; consequently, the residual current decreases with increasing surfactant concentration.

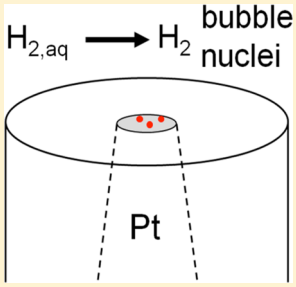

SECTION: Liquids; Chemical and Dynamical Processes in Solution

The presence of nano- or microgas bubbles formed on hydrophobic solid surfaces has been supported by direct imaging including atomic force microscopy (AFM),[1,2] total internal reflection fluorescence microscopy,[3] and high-speed photography.[4] Compelling evidence for nanobubble formation also comes from measurement of quartz crystal microbalance,[5] attenuated total internal reflection infrared spectroscopy,[6] and potential/current fluctuations at the electrode surface.[7] These gas bubbles may alter the interfacial properties, for example, surface forces, lubrication, and adsorption, and have significant implications including nanobubble cleaning[8] and colloidal particle stabilization.[9] Experimentally, nanobubbles can be efficiently produced using solvent-exchange,[3,6,10] pressure release,[11] heating,[12] and water electrolysis.[2,13,14] It has been proposed that interfacial nanobubbles result from a supersaturation of gas at the interface.[15,16] However, Seddon et al.[17] reported that supersaturation is not necessary for bubble nucleation. Despite extensive studies on gas nanobubbles, the mechanisms underlying the nucleation, formation, and stability of nanobubbles remain poorly understood.

Nucleation theories have been developed to understand these experiments. Homogenous bubble nucleation involves nucleation in the liquid bulk and requires a high supersaturation.[15,18] Heterogeneous nucleation is more likely to describe bubble formation at an electrode surface.[15,19] The rate J (s^{-1}) of heterogeneous nucleation of bubbles from a supersaturated solution on a surface can be estimated by[20]

$$J = C \exp\left(\frac{-16\pi\gamma^3\Phi(\theta)}{3kT(\sigma P')^2}\right) \quad (1)$$

where C (s^{-1}) can be treated as constant, γ (N/m) is the liquid surface tension, σ is the supersaturation of the gas in the liquid ($= c/c_{saturation} - 1$, where c and $c_{saturation}$ are, respectively, the concentration and saturation concentration of the gas at a given pressure), and P' (Pa) is the applied pressure at which nucleation takes place. Φ (dimensionless) is a function of the contact angle, θ (deg), and is given by

$$\Phi(\theta) = \frac{1}{4}(1 + \cos\theta)^2(2 - \cos\theta) \quad (2)$$

Thus, the bubble contact angle should be determined by the solid–liquid (γ_{SL}), solid–vapor (γ_{SV}), and liquid–vapor (γ_{LV}) surface tension from the Young equation ($\gamma_{SL} = \gamma_{SV} + \gamma_{LV}\cos\theta$). A hydrophobic solid surface usually results in a small gas bubble contact angle. The threshold bubble nucleation conditions can be described by the supersaturation concentration of a dissolved gas in the solution. According to the literature reported,[15,19,21] there are large discrepancies between the threshold supersaturation predicted theoretically and those indicated by empirical observations.

AFM has been used to investigate the shapes of nanobubbles in liquids, but the tip–bubble interaction potentially affects the morphology of the surface bubbles during scanning, and it is still difficult to observe the gas evolution at the early stages. Optical techniques do not probe sufficiently small length scales to characterize nanobubbles. Electrochemistry, however, in addition to being used to produce gas nanobubbles at the

Received: September 7, 2014
Accepted: September 26, 2014
Published: September 26, 2014

   dx.doi.org/10.1021/jz501898r | J. Phys. Chem. Lett. 2014, 5, 3539–3544

electrode surface,[2,14] can probe bubble nucleation, growth, and stability. We previously reported electrogeneration of single H_2 nanobubbles in sulfuric acid at Pt disk electrodes of radii less than ~50 nm.[22] As the electrode potential is scanned negative, the current from H_2 generation begins to increase but then suddenly decreases, indicating the formation of a nanobubble at the electrode surface that partially blocks the proton transfer to the electrode surface. In this report, we focus on the mechanism of bubble nucleation and the effect of various surfactants on nucleation and stabilization.

Sulfuric acid (96.2%, ACS grade), hydrochloric acid (37%, ACS grade), phosphoric acid (85%, ACS grade), poly(ethylene glycol)(300 g/mol), surfactants Triton X-100, tetraethylene glycol monododecyl ether (TEGME), and cetyltrimethylammonium bromide (CTAB) were used as received. Ferrocene (Fc) was purified by sublimation. All aqueous solutions were prepared from deionized water (18.2 MΩ·cm). Pt nanodisk electrodes were fabricated according to previously reported procedures from our laboratory.[23] The radii of the nanodisk electrodes, a, were determined from the voltammetric steady-state diffusion-limited current, i_d, for the oxidation of Fc ($Fc \rightarrow Fc^+ + e^-$) dissolved in acetonitrile containing 0.10 M tetrabutylammonium hexafluorophosphate ($TBAPF_6$). The radii were calculated using the following equation

$$i_d = 4nFD_{Fc}C^*_{Fc}a \quad (3)$$

where D_{Fc} (cm^2/s) and C^*_{Fc} (mol/cm^3) are the diffusion coefficient and the bulk concentration of Fc, respectively, and n is the number of electrons transferred per molecule (= 1 for Fc oxidation). The experimental steady-state voltammograms recorded for measuring the electrode radii are presented in the Supporting Information (Figure S1), and the literature value of $D_{Fc} = 2.4 \times 10^{-5}$ cm^2/s for Fc in acetonitrile[24] was used to compute values of a. A Dagan Cornerstone ChemClamp potentiostat and a Pine RDE4 (used as the waveform generator) were interfaced to a computer through a PCI data acquisition card (National Instruments) to collect the $i-V$ data. A Ag/AgCl (3 M NaCl) electrode was used as the counter/reference electrode.

Figure 1a shows typical cyclic voltammograms recorded at Pt nanodisk electrodes of different radii immersed in 0.5 M H_2SO_4 (scan rate = 100 mV/s). When the voltage is scanned negative of ~−0.25 V versus Ag/AgCl, corresponding to the thermodynamic potential E^0 for the reaction $2H^+ + 2e^- \leftrightarrow H_2$, the current associated with electrogeneration of H_2 increases rapidly until reaching a peak value, i^p_{nb}, and then suddenly drops to a low residual current. We previously ascribed this characteristic waveshape to the formation of a single nanobubble at the electrode surface. The residual current after a nanobubble is formed corresponds to the rate of H_2 electrogeneration at the electrode surface required to balance the H_2 diffusive outflux from the bubble into the solution. For a 2.5 nm radius electrode, the peak current (i^p_{nb}) at which a bubble nucleates is ~2.9 nA, while for a 22 nm radius electrode, i^p_{nb} increases to ~13.9 nA. The i^p_{nb} value for a given electrode is independent of the scan rate from 10 mV/s to 10 V/s (Figure S2a in the Supporting Information), indicating that the H_2 concentration profile around the electrode surface reaches a steady state within this range of voltammetric scan rate.

As previously reported, the appearance of a sharp peak in the voltammetric response occurs only at H^+ concentrations above ~0.5 M. Below this critical value, the voltammetic response of the nanodisk electrode displays a sigmoidal shape that is

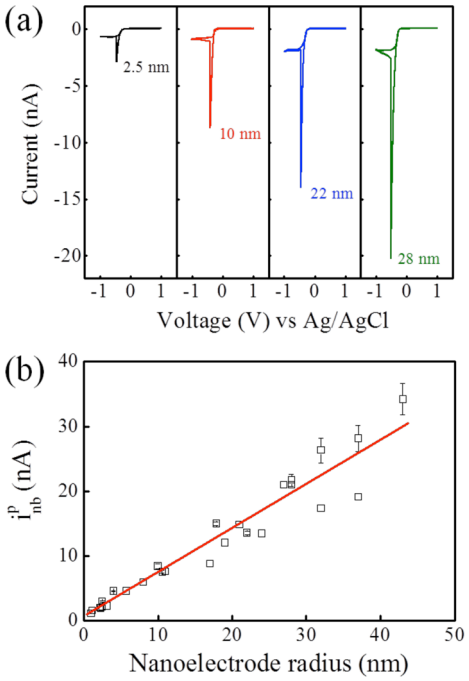

Figure 1. (a) Typical $i-V$ responses of Pt nanoelectrodes with radii of 2.5, 10, 22, and 28 nm in 0.5 M H_2SO_4 at a scan rate of 100 mV/s. (b) Nanobubble peak current i^p_{nb} as a function of nanoelectrode radii. Representative error bars are given for some of the electrodes.

characteristic of a diffusion-limited response without interference of a phase transition. Figure S3a in the Supporting Information shows voltammograms recorded at a 25 nm-radius Pt nanodisk in HCl solution below the critical concentration (0.05, 0.10, and 0.20 M), from which a value of D for H^+ equal to 8.1×10^{-5} cm^2/s was estimated in Figure S3c in the Supporting Information (literature value = 9.3×10^{-5} cm^2/s).[25] Above the critical concentration of ~0.5 M, the voltammetric response is nearly independent of HCl concentration (Figure S3b in the Supporting Information), displaying a concentration-independent value of i^p_{nb}. An essentially identical dependence of the voltammetric response on H_2SO_4 concentration, below and above the critical concentration, was presented in our previous report. In summary, at low H^+ concentrations, the corresponding concentration of electrogenerated H_2 at the electrode surface fails to achieve the value required for bubble nucleation, while at a higher H^+ concentration, a sufficient concentration of H_2 molecules nucleates a nanobubble, as indicated by the precipitous drop in current when the current reaches the value i^p_{nb}.

Because the voltammetric current arises from the reduction of H^+, the steady-state H_2 concentration directly at the electrode surface can be estimated using the expression

$$i^p_{nb} = 4nFD_{H_2}C^s_{H_2,critical}a \quad (4)$$

where D_{H_2} is the diffusivity of H_2 (4.5×10^{-5} cm^2/s)[25] and n is the number of electrons transferred per formation of a H_2 molecule ($n = 2$). Equation 4 relates the surface concentration of H_2, $C^s_{H_2,critical}$, to the peak current, i^p_{nb}, at the moment just prior to bubble nucleation. The slope from the linear plot of i^p_{nb} versus a (Figure 1b) yields the critical surface H_2 concentration $C^s_{H_2,critical}$ of 0.25 M, that is, the concentration of H_2 that leads to the formation of a stable bubble. Implicit in our analysis using

dx.doi.org/10.1021/jz501898r | J. Phys. Chem. Lett. 2014, 5, 3539−3544

eq 4 is the assumption that the concentration of electrogenerated H_2 is uniform across the electrode surface. This condition is fulfilled when the reduction of H^+ is limited primarily by diffusion and not by electron-transfer kinetics or ohmic potential drop. The shape of the rising part of the voltammetric wave, prior to the nucleation of the bubble, and the proximity of the rising current to E^0 for the H_2/H^+ couple are both consistent with a diffusion-controlled response, justifying the use of eq 4 in computing values of $C^s_{H_2,critical}$.

We find that $C^s_{H_2,critical}$ is independent of electrode radii up to 50 nm, above which a sharp nucleation peak in the voltammetric response is not observed. Considering the saturation concentration of H_2 in H_2O at 1 atm and room temperature to be ~0.8 mM, the measured surface concentration is ~310 times the saturation of H_2 at bubble nucleation. In the pressure release method, where gases are first dissolved in the solution at a high pressure before applying decompression, the supersaturation required to cause bubble nucleation in aqueous solution varied from 1.3 to 320, depending on the gas species.[19,26] For H_2 gas generated from rapid decomposition of $NaBH_4$ in water, the threshold for bubble nucleation was reported to be ~80 times saturation.[27] However, in the conventional electrochemistry method, where larger bubble formation was recorded using the cinemicrography, the supersaturation values for nucleation in H_2SO_4 solutions were reported much lower, for example, 8 to 24 by Westerheide et al.,[28] 1.54 to 19.9 by Glas et al.[29] at a Pt microelectrode, and 9 to 16 by Dapkus et al.[13] at a mercury electrode. These differences may be due to different properties of the larger microelectrodes and our nanoelectrodes including the effective surface areas for electrochemical reaction, surface properties, and electric field.

Single nanobubble nucleation at a Pt electrode surface was studied using different acids as the source of H^+. Figure 2 shows

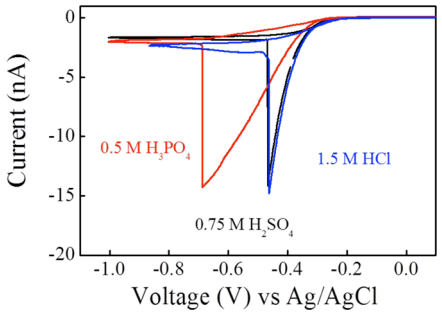

Figure 2. Typical $i-V$ responses of an 18 nm radius Pt nanoelectrode immersed in different acid solutions: 0.5 M H_3PO_4, 0.75 M H_2SO_4, and 1.5 M HCl at a scan rate of 100 mV/s.

typical cyclic voltammograms for an 18 nm radius Pt electrode immersed in 1.5 M HCl, 0.75 M H_2SO_4, and 0.5 M H_3PO_4. As previously noted, we find that i^p_{nb} = ~15 nA is independent of the acid species, indicating that the nucleation supersaturation is independent of the proton source. Note that HCl and H_2SO_4 are strong acids, while H_3PO_4 is a weak acid. The calculated bulk proton concentrations in equilibrium for HCl, H_2SO_4, and H_3PO_4 at the previously listed concentrations are 1.50, 0.83, and 0.057 M, respectively. Thus, while the HCl and H_2SO_4 solutions provide sufficient free H^+ to nucleate a nanobubble at low overpotential, the H_3PO_4 does not. Thus, the cyclic voltammograms recorded in the HCl and H_2SO_4 are quite similar, while that for the H_3PO_4 is drawn out, resulting in nucleation at a more negative potential but at the same value of i^p_{nb}. A drawn-out voltammetric response, similar to that observed in the H_3PO_4 solution, is also observed in 1.5 M acetic acid (see Figure S4 in the Supporting Information). This is expected because dissociation of a weak acid requires a more negative voltage to drive the pre-equilibrium dissociation of the acid prior to proton reduction.[30−33]

Contamination has been previously invoked to explain the long lifetime of interfacial nanobubbles.[34] The hypothesis suggests that the presence of surface contaminant at the bubble/solution interface increases the bubble stability by decreasing the gas transfer rate across the bubble/solution interface. Surface contaminant also reduces the interfacial tension and bubble contact angle. The addition of surfactant was reported to remove and solubilize the pinned contaminant, and disappearance of the bubbles in the presence of SDS (at 5 times the critical micelle concentration (cmc)) was explained in terms of the loss of the stabilizing molecules at the air−water interface. This hypothesis has been partially supported by experiments by Lüderitz et al., who observed nanobubbles formation on silicon oxide surface at low CTAB concentration (0.05 mM to 0.4 mM) but detected no bubbles at concentration 0.5 mM upward.[35] In contrast, using the same standard solvent-exchange method for nanobubble formation and tapping-mode atomic force microscopy for detection, Zhang et al.[36] demonstrated that surfactants (SDS) have little effect on the stabilization of nanobubbles. These contradictory results prompted us to investigate the effects of surfactant molecules on H_2 bubble nucleation and stabilization at the nanodisk electrodes.

In preliminary experiments, the addition of common salts, for example, KCl, Na_2SO_4, and sodium citrate, to the H_2SO_4 solution at a concentration of 10 mM had no influence on the shape of the voltammetric response relative to that obtained in the absence of salts. Similarly, poly(ethylene glycol) (400 g/mol) added to the H_2SO_4 solution had very little effect on bubble nucleation at a 10 nm radius electrode, as shown in Figure 3a. However, significant differences were observed when amphiphilic surfactants were added to the solution. When nonionic surfactant molecules that contain both a hydrophilic ethylene glycol chain and a hydrophobic alkyl chain were added to the acid solution, the cyclic voltammogram displayed new characteristics. Figure 3b,c shows that in the presence of 0.10 mg/mL Triton X-100 or tetraethylene glycol monododecyl ether (TEGME) in 0.5 M H_2SO_4 solution the nanobubble peak currents decrease from 27.5 to 19.6 nA for a 32 nm radius electrode and from 12.3 nA to 7.7 nA for a 12 nm radius electrode, respectively. Additionally, the magnitude of the residual current after a nanobubble is formed is significantly reduced. Finally, upon the surfactant addition, the potentials corresponding to bubble nucleation shift negative compared with that in the absence of surfactant. These altered characteristics of the cyclic voltammograms were also observed for another ionic surfactant CTAB, as shown in Figure 3d, where the peak current decreases from 13.9 to 8.1 nA for a 22 nm radius electrode and the residual current at −1.0 V decreases from 2.0 to 0.2 nA after 0.10 mg/mL CTAB is introduced into the H_2SO_4 solution.

It is known that presence of surfactant can reduce the surface tension of the solution. According to the literature,[37] γ of water decreases from 0.072 to 0.033 N/m when Triton X-100 is present at 0.10 mg/mL. As suggested by eq 1, the rate of

dx.doi.org/10.1021/jz501898r | J. Phys. Chem. Lett. 2014, 5, 3539−3544

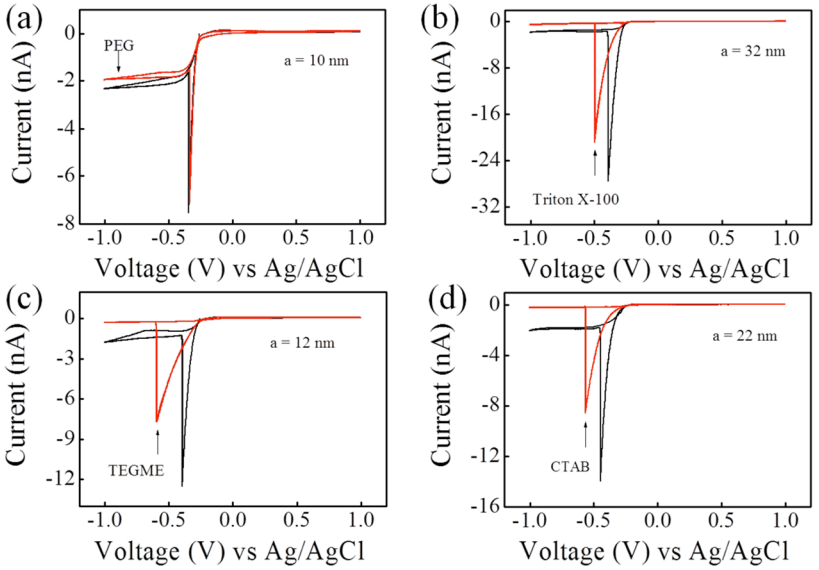

Figure 3. *i*−*V* responses of (a) a 10 nm radius Pt disk nanoelectrode with (red) and without (black) polyethylene glycol (PEG 300), (b) a 32 nm radius Pt disk nanoelectrode with (red) and without (black) surfactant Triton X-100, (c) a 12 nm radius Pt nanoelectrode with (red) and without (black) surfactant tetraethylene glycol monododecyl ether (TEGME), and (d) a 22 nm radius Pt nanoelectrode with (red) and without (black) surfactant cetyltrimethylammonium bromide (CTAB) in 0.5 M H_2SO_4 at scan rate = 100 mV/s. The mass concentration for PEG 300, Triton X-100, TEGME, and CTAB in the 0.5 M H_2SO_4 is the same, 0.10 mg/mL.

bubble nucleation is very sensitive to γ, increasing as $\exp(-\gamma^3)$. Thus, a decrease in γ would be expected to lead to H_2 nanobubble nucleation at a lower H_2 supersaturation, consistent with the observed reduction of peak current in the presence of surfactants in the acid solution.

As has been previously noted, the residual current indicates the kinetic balance of H_2 electrogeneration at the electrode surface (that is covered by the bubble) with the H_2 diffusive outflux into the solution.[22] We estimated from the magnitude of i_{nb}^r and using finite-element simulations of the diffusive transport of H^+ that the H_2 nanobubble covers the vast majority of the Pt surface (>99%). However, we find that i_{nb}^r shows little correlation with the nanoelectrode radii (see Figure S5 in the Supporting Information). At the moment, we do not completely understand why i_{nb}^r varies significantly for different electrodes with similar radii but speculate that small differences in the electrode shape and surface smoothness resulting from polishing during electrode preparation influence how much of the electrode surface remains exposed and is available for H^+ reduction. However, we emphasized that i_{nb}^r values are very reproducible for a specific Pt nanoelectrode, once prepared, based on repeated independent bubble formation experiments.

After a nanobubble forms at the electrode surface, amphiphilic surfactant molecules would favorably concentrate at the H_2 bubble/liquid interface, thereby reducing the interfacial tension and also hindering H_2 diffusion from the gas bubble into the solution. Additionally, according to the Young−Laplace equation

$$\Delta p = p_{in} - p_{out} = \frac{2\gamma}{r_{nb}} \quad (5)$$

reduction of surface tension decreases the inner pressure of nanobubble and subsequently slows down the dissolution of H_2 into the solution based on Henry's law. Considering the above two effects, a lower rate of H_2 electrogeneration (or residual current) is needed to balance the H_2 outflux; thus, the residual current is anticipated to decrease, as experimentally observed upon the addition of surfactants. Finally, the shift of peak potential to negative is also understandable in terms of the physisorption of surfactants at Pt surface and inhibition of electron transfer (proton reduction) at the electrode surface.[38−40] To produce the current (and H_2 surface concentration) needed to drive bubble nucleation, the potential needs to be scanned further negative to overcome the sluggish electron transfer.

To confirm the effect of surfactant molecules on the bubble nucleation and stability, we varied the concentration of CTAB from 0.0001 to 0.20 mg/mL below the cmc (0.36 mg/mL for CTAB) in acid solution. Figure S6 in the Supporting Information presents cyclic voltammograms for a 9 nm radius electrode immersed in 0.5 M H_2SO_4 at various CTAB mass concentrations. It is found that as the CTAB concentration increases, the peak current decreases, and voltage corresponding to the peak current shifts negative. After the measurements in the presence of CTAB, the electrode was carefully rinsed with copious amounts of ethanol and water. The cyclic voltammgrams for the cleaned electrode in 0.5 M H_2SO_4 show very similar characteristics as the pristine one, indicating that the reduction of peak current and residual current are due to the surfactants in the acid solution. The peak current as a function of CTAB concentration are shown in Figure 4a, while the residual current is presented in Figure 4b, for four different Pt electrodes with radius of 2.5, 4, 9, and 22 nm. i_{nb}^p decreases steadily with increasing CTAB concentration for all electrodes, regardless of radius. The residual current, i_{nb}^r, after a bubble is formed decreases as the CTAB concentration increases and levels off at ~5 × 10^{-3} mg/mL, indicating that CTAB molecules accumulating at the bubble interface reach a saturated level. It is surprising to find that the i_{nb}^r values at high CTAB concentrations are quite similar for electrodes with different radii. Further quantitative analysis of the residual current is not attempted because little is known about how the surfactant molecules impede the H_2 interfacial transfer.

dx.doi.org/10.1021/jz501898r | J. Phys. Chem. Lett. 2014, 5, 3539−3544

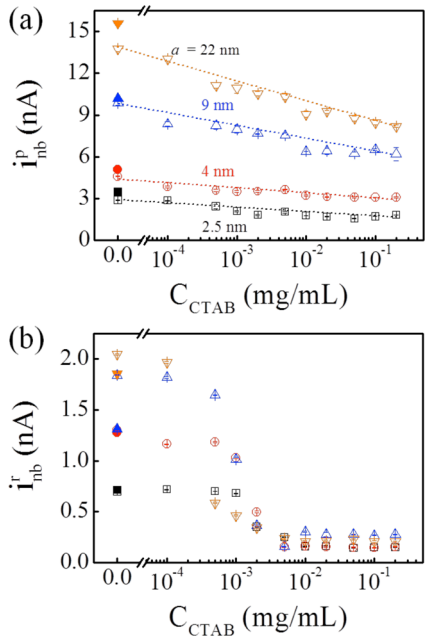

Figure 4. Cetyltrimethylammonium bromide (CTAB) concentration dependence of (a) nanobubble peak current, i^{p}_{nb}, and (b) nanobubble residual current, i^{r}_{nb}, at −1.0 V for disk nanoelectrodes with radii of 2.5, 4, 9, and 22 nm in 0.5 M H_2SO_4 at a scan rate of 100 mV/s. The filled symbols represent i^{p}_{nb} and i^{r}_{nb} for the cleaned electrodes after surfactant experiment, which are close to the values for pristine electrodes in 0.5 M H_2SO_4.

In summary, from the electrode radius dependence of nanobubble peak current (Figure 1b), we find that the H_2 supersaturation concentration at the electrode surface corresponding the nanobubble nucleation is ∼310 times larger than the saturation value at room temperature and pressure. Such a value is much higher than that reported for H_2 bubble nucleation at a Pt microelectrode or mercury electrode. This supersaturation for H_2 bubble nucleation is found to be independent of the proton source, as long as the proton supply is sufficient to produce high H_2 concentration at the electrode surface. We further systematically investigate the effect of surfactants (Triton X-100, TEGME, and CTAB) on the bubble nucleation and stability. Both nonionic surfactants and the ionic surfactants promote the nucleation at a lower level of supersaturation and further stabilize the nanobubbles, that is, reduce the nanobubble peak current and residual current. Such a finding is understandable from classic heterogeneous nucleation theory, which predicts that decreasing the liquid surface tension reduces the free-energy change for bubble nucleation. We speculate that the decrease in the residual current that is observed after a nanobubble is formed is due to the accumulation of surfactant molecules at gas−liquid interface, impeding the H_2 outflux to the solution. While electrochemistry of single nucleation events using nanoelectrodes provides a unique way to study nanobubbles, the shape of single nanobubbles studied here is poorly understood. We are currently working toward imaging individual H_2 nanobubble at Pt nanoelectrodes using AFM.

■ ASSOCIATED CONTENT

Ⓢ Supporting Information

Characterization of Pt nanodisk electrodes. Voltammetric responses of a 9 nm Pt electrode in 0.5 M H_2SO_4 in the absence and presence of CTAB at different scan rates. Voltammetric responses of a 25 nm Pt electrode in HCl solution with different proton concentrations. Voltammetric response of a 8 nm Pt electrode in 1.5 M acetic acid. Dependence of nanobubble residual current on nanoelectrode radii. Voltammetric responses of a 9 nm Pt electrode in 0.5 M H_2SO_4 with different concentrations of CTAB in the solution. This material is available free of charge via the Internet at http://pubs.acs.org.

■ AUTHOR INFORMATION

Corresponding Author

*E-mail: white@chem.utah.edu.

Notes

The authors declare no competing financial interest.

■ ACKNOWLEDGMENTS

This work was supported by the Office of Naval Research.

■ REFERENCES

(1) Yang, S.; Dammer, S. M.; Bremond, N.; Zandvliet, H. J. W.; Kooij, E. S.; Lohse, D. Characterization of Nanobubbles on Hydrophobic Surfaces in Water. *Langmuir* **2007**, *23*, 7072−7077.

(2) Zhang, L.; Zhang, Y.; Zhang, X.; Li, Z.; Shen, G.; Ye, M.; Fan, C.; Fang, H.; Hu, J. Electrochemically Controlled Formation and Growth of Hydrogen Nanobubbles. *Langmuir* **2006**, *22*, 8109−8113.

(3) Chan, C. U.; Ohl, C.-D. Total-Internal-Reflection-Fluorescence Microscopy for the Study of Nanobubble Dynamics. *Phys. Rev. Lett.* **2012**, *109*, 174501.

(4) Fernández, D.; Maurer, P.; Martine, M.; Coey, J. M. D.; Möbius, M. E. Bubble Formation at a Gas-Evolving Microelectrode. *Langmuir* **2014**, 10.1021/la500234r.

(5) Zhang, X. H. Quartz Crystal Microbalance Study of the Interfacial Nanobubbles. *Phys. Chem. Chem. Phys.* **2008**, *10*, 6842−6848.

(6) Zhang, X. H.; Quinn, A.; Ducker, W. A. Nanobubbles at the Interface between Water and a Hydrophobic solid. *Langmuir* **2008**, *24*, 4756−4764.

(7) Gabrielli, C.; Huet, F.; Keddam, M. Potential Drops Due to an Attached Bubble on a Gas-Evolving Electrode. *J. Appl. Electrochem.* **1989**, *19*, 617−629.

(8) Liu, G.; Wu, Z.; Craig, V. S. J. Cleaning of Protein-Coated Surfaces Using Nanobubbles: An Investigation Using a Quartz Crystal Microbalance. *J. Phys. Chem. C* **2008**, *112*, 16748−16753.

(9) Jin, F.; Gong, X.; Ye, J.; Ngai, T. Direct Measurement of the Nanobubble-Induced Weak Depletion Attraction between a Spherical Particle and a Flat Surface in an Aqueous Solution. *Soft Matter* **2008**, *4*, 968−971.

(10) Lhuissier, H.; Lohse, D.; Zhang, X. Spatial Organization of Surface Nanobubbles and Its Implications in Their Formation Process. *Soft Matter* **2014**, *10*, 942−946.

(11) Gerth, W. A.; Hemmingsen, E. A. Heterogeneous Nucleation of Bubbles at Solid Surfaces in Gas-Supersaturated Aqueous Solutions. *J. Colloid Interface Sci.* **1980**, *74*, 80−89.

(12) Witharana, S.; Phillips, B.; Strobel, S. Bubble Nucleation on Nano-to Micro-Size Cavities and Posts: An Experimental Validation of Classical Theory. *J. Appl. Phys.* **2012**, *112*, 064904.

(13) Dapkus, K. V.; Sides, P. J. Nucleation of Electrolytically Evolved Hydrogen at an Ideally Smooth Electrode. *J. Colloid Interface Sci.* **1986**, *111*, 133−151.

(14) Yang, S.; Tsai, P.; Kooij, E. S.; Prosperetti, A.; Zandvliet, H. J. W.; Lohse, D. Electrolytically Generated Nanobubbles on Highly Orientated Pyrolytic Graphite Surfaces. *Langmuir* **2009**, *25*, 1466−1474.

(15) Jones, S. F.; Evans, G. M.; Galvin, K. P. Bubble Nucleation from Gas Cavities—A Review. *Adv. Colloid Interface Sci.* **1999**, *80*, 27−50.

(16) Craig, V. S. J. Very Small Bubbles at Surfaces—the Nanobubble Puzzle. *Soft Matter* **2011**, *7*, 40−48.

(17) Seddon, J. R. T.; Kooij, E. S.; Poelsema, B.; Zandvliet, H. J. W.; Lohse, D. Surface Bubble Nucleation Stability. *Phys. Rev. Lett.* **2011**, *106*, 056101.
(18) Weathersby, P. K. Homogeneous Nucleation of Gas Bubbles in Vivo. *J. Appl. Physiol.: Respir., Environ. Exercise Physiol.* **1982**, *53*, 940−946.
(19) Lubetkin, S. D. Why Is It Much Easier to Nucleate Gas Bubbles than Theory Predicts? *Langmuir* **2003**, *19*, 2575−2587.
(20) Lubetkin, S.; Blackwell, M. The Nucleation of Bubbles in Supersaturated Solutions. *J. Colloid Interface Sci.* **1988**, *126*, 610−615.
(21) Hemmingsen, E. A. Spontanous Formation of Bubbles in Gas-Supersaturated Water. *Nature* **1977**, *267*, 141−142.
(22) Luo, L.; White, H. S. Electrogeneration of Single Nanobubbles at Sub-50-nm-Radius Platinum Nanodisk Electrodes. *Langmuir* **2013**, *29*, 11169−11175.
(23) Zhang, B.; Zhang, Y.; White, H. S. The Nanopore Electrode. *Anal. Chem.* **2004**, *76*, 6229−6238.
(24) Kuwana, T.; Bublitz, D. E.; Hoh, G. Chronopotentiometric Studies on the Oxidation of Ferrocene, Ruthenocene, Osmocene and Some of Their Derivatives. *J. Am. Chem. Soc.* **1960**, *82*, 5811−5817.
(25) Cussler, E. L. *Diffusion: Mass Transfer in Fluid Systems*, 2nd ed.; Cambridge University Press: New York, 1997.
(26) Gerth, W. A.; Hemmingsen, E. A. Gas Supersaturation Thresholds for Spontaneous Cavitation in Water with Gas Equilibration Pressures up to 570 atm. *Z. Naturforsch., A* **1976**, *31*, 1711−1716.
(27) Rubin, M. B.; Noyes, R. M. Measurements of Critical Supersaturation for Homogeneous Nucleation of Bubbles. *J. Phys. Chem.* **1987**, *91*, 4193−4198.
(28) Westerheide, D. E.; Westwater, J. W. Isothermal Growth of Hydrogen Bubbles during Electrolysis. *AIChE J.* **1961**, *7*, 357−362.
(29) Glas, J. P.; Westwater, J. W. Measurements of the Growth of Electrolytic Bubbles. *Int. J. Heat Mass Transfer* **1964**, *7*, 1427−1443.
(30) Daniele, S.; Baldo, M. A.; Simonetto, F. Assessment of Linearity between Steady-State Limiting Current and Analytical Concentration of Weak Acids in the Reaction of Hydrogen Evolution. *Anal. Chim. Acta.* **1996**, *331*, 117−123.
(31) Daniele, S.; Lavagnini, I.; Baldo, M. A.; Magno, F. Steady State Voltammetry at Microelectrodes for the Hydrogen Evolution from Strong and Weak Acids under Pseudo-First and Second Order Kinetic Conditions. *J. Electroanal. Chem.* **1996**, *404*, 105−111.
(32) Canhoto, C.; Matos, M.; Rodrigues, A.; Geraldo, M. D.; Bento, M. F. Voltammetric Analysis of Weak Acids with Microelectrodes. *J. Electroanal. Chem.* **2004**, *570*, 63−67.
(33) Stojek, Z.; Ciszkowska, M.; Osteryoung, J. G. Self-Enhancement of Voltammetric Waves of Weak Acids in the Absence of Supporting Electrolyte. *Anal. Chem.* **1994**, *66*, 1507−1512.
(34) Ducker, W. A. Contact Angle and Stability of Interfacial Nanobubbles. *Langmuir* **2009**, *25*, 8907−8910.
(35) Lüderitz, L. A. C.; von Klitzing, R. Scanning of Silicon Wafers in Contact with Aqueous CTAB Solutions below the CMC. *Langmuir* **2012**, *28*, 3360−3368.
(36) Zhang, X.; Uddin, M. H.; Yang, H.; Toikka, G. Effects of Surfactants on the Formation and the Stability of Interfacial Nanobubbles. *Langmuir* **2012**, *28*, 10471−10477.
(37) Makievski, A. V.; Fainerman, V. B.; Joos, P. Dynamic Surface Tension of Micellar Triton X-100 Solutions by the Maximum-Bubble-Pressure Method. *J. Colloid Interface Sci.* **1994**, *166*, 6−13.
(38) Ohsaka, T.; Abe, Y.; Yoshida, T. Adsorption of Organic Polymers on Platinum Electrode. *Bull. Chem. Soc. Jpn.* **1973**, *46*, 1324−1973.
(39) Safonova, T. Y.; Smirnova, N. V.; Petrii, O. A. Adsorption of Polyethylene Glycol on Platinum Electrode from Acidic Solutions. *Russ. J. Electrochem.* **2006**, *42*, 995−1000.
(40) Stickney, J. L.; Soriaga, M. P.; Hubbard, A. T. A Survey of Factors Influencing the Stability of Organic Functional Groups Attached to Platinum Electrodes. *J. Electroanal. Chem.* **1981**, *125*, 73−88.